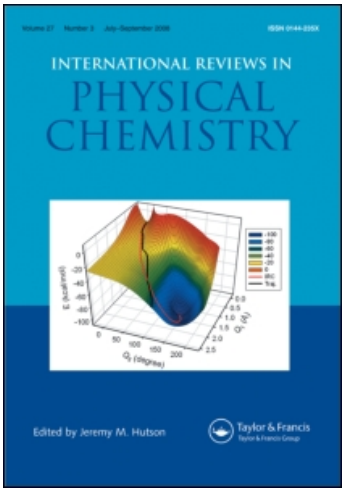

International Reviews in Physical Chemistry
Publication details, including instructions for authors and subscription information:
http://www.informaworld.com/smpp/title~content=t713724383

Structure and chemical modification in oxide glasses

J. W. Zwanziger

Online publication date: 26 November 2010

To cite this Article Zwanziger, J. W.(1998) 'Structure and chemical modification in oxide glasses', International Reviews in Physical Chemistry, 17: 1, 65 — 90
To link to this Article: DOI: 10.1080/014423598230171
URL: http://dx.doi.org/10.1080/014423598230171

INTERNATIONAL REVIEWS IN PHYSICAL CHEMISTRY, 1998, VOL. 17, NO. 1, 65–90

Structure and chemical modification in oxide glasses

by J. W. ZWANZIGER

Department of Chemistry, Indiana University, Bloomington, IN 47405, USA

The structure of oxide glass consists of relatively well defined oxide polyhedra, with significant disorder in the linkages between these groups. We review recent progress in understanding these structures, including the length scales over which they exist, and how they may be modified chemically. We discuss two primary experimental methods: nuclear magnetic resonance (NMR) spectroscopy and neutron diffraction. We explain how several methods for achieving high resolution in solid-state NMR may be applied to glasses, and how the data from NMR and neutron diffraction may be used together to generate large models that are consistent with both sets. Specific examples are used to illustrate these points, including glasses based on borates, phosphates and tellurites.

1. Introduction

Glasses have no long-range order, but their structure at shorter ranges is well defined, if complex. We shall discuss glass structure using the terminology of Elliott [1, 2], identifying three length scales: short, intermediate and long range. Short-range order persists over one or two chemical bonds and consists of the basic polyhedra and coordination shells making up the glass. Intermediate-range order extends from (roughly) 5 to 20 Å and describes how the polyhedra are linked, the clustering or avoidance of cations, and so forth. Certain hints of structures persisting beyond about 20 Å, which is the cut-off to long-range order, have been described [3], but essentially glass is isotropic on this length scale and we shall not discuss such structures here.

Fundamental interest in these structures stems from the desire to understand the glass transition, which is surely one of the least-understood transitions in physical science, particularly in light of the more or less common-place nature of glass. Glass is formed conventionally by freezing a liquid faster than it can crystallize, meaning that thermal energy is removed from the melt on a time scale faster than the liquid structure can settle into a crystalline array. The melt is then presumably trapped in a local free-energy minimum, without enough thermal energy to escape the barriers. This picturesque description of the glass transition is meant to be only heuristic, in particular because it posits glass formation as an essentially thermodynamic event. There are currently several rather sharply opposed theories of the glass transition, some of which are explicitly kinetic, rather than thermodynamic [4–7]. Here we shall discuss the structure of the glass *after* it has formed but not discuss further the transition itself, except to point out that the structures that we determine reflect the transition indirectly, as they are the structures that froze in as the time scale of dynamics became long.

The technological interest in glass structure arises from the impact that it has on the many uses of glass. For example, some glasses show remarkably high ionic conductivity, on par with that of dilute aqueous salt solutions [8, 9]. This phenomenon is quite intriguing, given that the glasses are otherwise hard brittle solids [10]. The electronic conductivity in these materials is still very low, making them candidates for all-solid-state batteries. The glass structure plays an important role in the conductivity

0144–235X/98 $12.00

of a particular composition, in that additives can be included which open up the glass matrix, allowing easier movement of otherwise trapped ions [8, 11, 12]. In order to exploit and understand this conductivity, it is essential to find which structures give rise to it and how they may be modulated.

Over the past several years, our laboratory has made progress in discovering the structure on both short- and intermediate-range order in several different glass systems. To accomplish this we used a variety of one- and two-dimensional nuclear magnetic resonance (NMR) experiments, neutron diffraction and modelling. Our results show how intermediate-range order arises in these different families and provides some answers to questions concerning how this order impacts the bulk properties of the glasses.

The purpose of this review is to explain the methods that we used to obtain these results, and to interpret the results in the context of current notions of glass structure and applications. We shall describe three glass systems: borates, phosphates and tellurites. All three are typical oxide glass-forming families, consisting of a network former (boron oxide (B_2O_3), phosphorus pentoxide (P_2O_5), and tellurium dioxide (TeO_2) respectively) and a modifier (alkali metal oxides in the borates and tellurites, silver oxide in the phosphates). Additionally, the silver phosphate ($AgPO_3$) glasses are further modified with the salt silver iodide (AgI). The standard view of the solid-state chemistry of such glasses is that the modifier acts to cleave network bonds, creating non-bridging oxygen (NBO) atoms as it does so. The salt is presumed to dissolve into the structure without causing any further bond breaking. We shall show that this paradigm, while qualitatively correct, gives only a gross picture of the structures of these families. In the silicates, in contrast, this view of the modification is essentially quantitative. The glasses considered here differ from silicates owing to the different bonding motifs favoured by the different main-group elements.

In the next section we shall explain the experimental methods used, concentrating on the NMR techniques and the modelling algorithm. The neutron diffraction methods that we use are fairly standard and will be reviewed very briefly. Then we describe the structural information that we have uncovered in some detail, for each system. In the borates we discuss the basic bonding pattern in pure B_2O_3 glass, and how already at this level intermediate-range order is an important feature. We then show how different elements in the glass are modified preferentially by the addition of alkali oxide. Then we discuss silver iodide–silver phosphate glasses and show how with a combination of silver and phosphorus NMR we could determine important details of the silver conduction process. Finally, in tellurites we show how NMR and neutron diffraction can be combined with reverse Monte Carlo modelling to generate uniform models of the glass structure, and how these models are used to analyse the origin of composition-dependent intermediate-range order in this system.

2. Experimental methods

2.1. *Nuclear magnetic resonance*

2.1.1. *Resolution of distinct sites*

NMR is an exceptional technique for probing the short-range structure of a material, whether solid or liquid. Chemically specific information can be obtained on the types of distinct atomic site, their relative occupancy and their connectivity, both through bond and through space. This information is usually easier to extract from liquid samples than from solid samples, because of the isotropic averaging on the experimental time scale. For solid samples, the anisotropy of spin interactions induces

additional inhomogeneous line broadening which obscures much of the desired information. This broadening can be controlled and even removed, however, by judicious modulation of the sample during the course of the experiment [13–15]. The point is that the full isotropic averaging present in a liquid is more than sufficient to remove the inhomogeneous broadenings, because the interactions that give rise to them transform not like tensors of all ranks, but only of a limited set [14].

For example, the chemical shift, which provides us with much of the basic chemical information about different sites, can be viewed as a Cartesian tensor coupling the angular momentum to the magnetic field [13]. This tensor can be profitably decomposed into its spherical components, which include a rank-0 term (the isotropic shift, observed in NMR experiments on liquids) and a rank-2 term. The latter term gives rise to inhomogeneous broadening but, owing to the transformational properties of rank-2 spherical tensors, full isotropic averaging is unnecessary to remove it. Rank-2 tensors transform under rotations in the same way as d orbitals and thus have an angular node at $\theta_m^{(2)} = \cos^{-1}(1/3^{1/2})$, the 'magic angle'. Rotating the sample about an axis fixed at an angle θ with respect to the external magnetic field modulates the rank-2 part of the chemical shift interaction such that it is scaled by $P_2(\cos\theta)$, where P_2 is the second Legendre polynomial; magic angle spinning (MAS) is achieved when $\theta = \theta_m^{(2)}$, because $P_2(\cos\theta_m^{(2)}) = 0$. Under these conditions the inhomogeneous broadening is removed. This is the well known MAS technique.

MAS NMR is of great utility in the study of polycrystalline solids, and also in the study of glass structure. Because the short-range order in glass is quite similar to that in crystalline materials, NMR remains an effective probe, although the resonances are broadened by the disorder. Thus line-narrowing techniques such as MAS retain their effectiveness, and MAS NMR has yielded significant information on the structure of a variety of glasses. It has been used in studies of silicates [16–18] and phosphates [19, 20] to show the types and concentrations of silicate and phosphate polyhedra present in the glass. Recently, extensions of MAS to several dimensions have appeared, which further facilitate studies of spin-$\frac{1}{2}$ nuclei in glass. These include off-angle-MAS correlation experiments [21], and variable-angle correlation spectroscopy [22–24], both of which yield high-resolution spectra correlated with structurally informative anisotropic shift dimensions.

The limitation of the MAS technique is that, while it is effective at removing inhomogeneous broadenings arising from rank-2 interactions, not all the significant anisotropic interactions are rank 2. The problematic interaction typically encountered is the quadrupole effect, which arises from the coupling between the non-spherical charge distribution in the nucleus and the electric field gradient generated by the surrounding electron distribution [25]. Spin-$\frac{1}{2}$ nuclei have strictly spherical charge distributions, so the important cases of ^{1}H, ^{13}C, ^{29}Si and ^{31}P are not subject to quadrupole interactions. However, about two thirds of the nuclei in the periodic table have spin greater than $\frac{1}{2}$, including ^{11}B, ^{17}O, ^{23}Na and ^{27}Al, all of which are important in glass science. Because the quadrupole interaction (for the above examples) is typically of strength 1–5 MHz, compared with Zeeman splittings of order 50–100 MHz and chemical shift anisotropy of 50–200 ppm (0.0025–0.02 MHz), the quadrupole effect is a significant perturbation which could render the NMR of such nuclei infeasible. This is in fact essentially the case for integer spins such as ^{14}N. For half-odd-integer spins, such as the four examples listed above, the quadrupole interaction has no effect on the resonance linewidth, at least to first order. In fact, this statement must be qualified, as follows: the selection rule for observation in NMR is $\Delta m = \pm 1$, where

m is the magnetic quantum number. The quadrupole interaction is bilinear in the nuclear angular momentum, which means that the transition frequency for the so-called central transition, between $m = \frac{1}{2}$ and $m = -\frac{1}{2}$, is unaffected by quadrupole effects. This fortunate circumstances arises owing to the bilinearity of the interaction, which causes the frequencies to depend on m^2; thus both m levels in the central transition shift but shift equally. The satellite transitions are inhomogeneously broadened in first order, although they can be observed under special circumstances; this forms the basis of the satellite transition spectroscopy technique [26]. Integer-spin quadrupolar nuclei have no transitions analogous to the central transition, making their observation difficult.

At second order in the quadrupole interaction, even the central transition is inhomogeneously broadened. Because the quadrupole interaction also transforms like a rank-2 spherical tensor, it might seem that this broadening can be removed by MAS. In fact, it could, at first order. However, the second-order effect is best viewed as arising from the recoupling of the rank-2 interaction with itself, which generates terms that transform like rank 0, rank 2 and rank 4 (the odd terms are absent owing to symmetry) [15]. Because the quadrupole interaction is so strong, even the second-order term is significant, imposing inhomogeneous linewidths in the range 10–30 kHz for the examples quoted above. These linewidths are sufficient to mask the desired chemical information. MAS averages away the rank-2 component, and some of the rank-4 term, but yields linewidths still some 5 kHz broad in typical cases. Because the rank-4 term, which transforms the same way as does a g orbital, has no orbital node coincident with that of the rank-2 term, spinning about a single axis alone cannot average away the second-order quadrupole anisotropy.

Over the last decade, several new methods have become available which accomplish for half-odd-integer quadrupole nuclei the type of resolution enhancement that MAS did for spin-$\frac{1}{2}$ systems. While none is as convenient to use as MAS, this will hopefully change as they are developed further. These new methods depend on modulating the space and spin degrees of freedom of the interactions in ways that average out both first- and second-rank interactions. Double rotation (DOR) is the most direct of these methods and works by spinning the sample about a *moving* axis [27–30]. The main sample holder rotates at about 1 kHz, about an axis at the $\theta_m^{(2)}$ magic angle. Within this holder, the sample is contained in a secondary holder which rotates *independently* of the main rotor, at an angle $\theta_m^{(4)}$ with respect to the main rotor axis, chosen such that $P_4(\cos\theta_m^{(4)}) = 0$. The inner rotor rotates at typically 5 kHz. The NMR experiment is then a simple pulse–acquire sequence, much like MAS. The spectrum contains the central transition frequencies, free of inhomogeneous broadening. However, because the outer rotor spins so slowly, the spectrum also contains a proliferation of spinning side bands, which complicates analysis (particularly of relative intensities). The experiment is also quite difficult to perform, and the equipment is specialized and costly.

Dynamic angle spinning (DAS) also requires a specialized probe but is mechanically easier to implement [29, 31–33]. In this experiment the sample spins again about a time-dependent axis, but now the time dependence is discrete rather than continuous. Spinner axis angles θ_1 and θ_2 are chosen to satisfy the simultaneous equations

$$P_2(\cos\theta_1) = -kP_2(\cos\theta_2), \tag{1}$$

$$P_4(\cos\theta_1) = -kP_4(\cos\theta_2), \tag{2}$$

where k is a positive constant. Because of the negative sign, the anisotropy acquired by

the signal during the evolution at θ_1 is cancelled by the anisotropy acquired during acquisition at θ_2, resulting in an echo which evolves with only the isotropic frequency components. The experiment is performed as a two-dimensional sequence, in which the indirect dimension corresponds to θ_1 evolution. Detection is carried out during θ_2 evolution, and the two periods are separated by a magnetization storage period during which the sample is reoriented from θ_1 to θ_2. The rotor spins at upwards of 5 kHz during the entire experiment, and it requires 20–40 ms to change the rotor orientation. This waiting time is the main limitation of this experiment, because in some cases the dipole coupling is sufficiently strong to quench the stored signal during the reorientation. DOR does not suffer from this limitation, but the two-dimensional nature of DAS has its own advantages, which we shall illustrate below.

Both DOR and DAS yield high-resolution spectra of distinct sites separated by their isotropic shifts. This shift contains the well known isotropic chemical shift, as in MAS, but additionally it includes a quadrupolar part, which arises from the second-order expansion of the quadrupole Hamiltonian. This point can be confusing, because the quadrupole Hamiltonian is traceless; so under isotropic averaging, as in liquids, no shift due to quadrupole coupling is possible. In the solid state, however, the system is static and it is most convenient to describe the interactions using static (Van Vleck) perturbation theory [34]. At first order, only the $m = 0$ component (which commutes with the Zeeman Hamiltonian) is present and, as noted above, gives no shift to the central transition. At second order, the rank-2 quadrupole is recoupled with itself, giving ranks 0–4; the rank-0 term is the second-order quadrupole shift. It takes the form (in parts per million):

$$\delta_{\mathrm{iso}}^{2\mathrm{Q}} = -\frac{3}{40}\left(\frac{e^2Qq/h}{\nu_0}\right)^2 \frac{I(I+1)-\frac{3}{4}}{I^2(2I-1)^2}\left(1+\frac{\eta^2}{3}\right)\times 10^6, \tag{3}$$

for a spin-I nucleus, Larmor frequency ν_0, quadrupole interaction e^2Qq/h and quadrupole asymmetry η. Note that it vanishes at high fields. The field dependence makes it possible to separate this term from the chemical shift, if DAS or DOR spectra are acquired at several field strengths.

Quite recently a third possibility to remove rank-2 broadenings has appeared, called multiple-quantum magic angle spinning (MQMAS) [35, 36]. This experiment is quite like DAS in spirit, but the two evolution periods differ not by spinning axis but by the coherence levels they use. In MQ MAS, a triple-quantum transition (nominally forbidden under direct excitation but achievable with long pulses and/or multiple pulses) is correlated with a single-quantum coherence during detection. The frequencies of the coherences are related by equations similar to equation (2), and an echo is obtained which again evolves at only the isotropic frequencies. The advantage of this experiment is that spinning at only the normal magic angle is required; so no specialized equipment is needed and the experiment is mechanically simple. The disadvantage is that excitation of the triple-quantum coherence is quite difficult and is particularly difficult to do in a quantitative way if there are multiple sites with different local environments. It is also difficult to perform on glasses, but initial results appear promising [37, 38].

2.1.2. *Measurement of site–site distances*

In addition to determining the nature and occupancy of binding sites in glass, NMR is useful for estimating the distances between sites. This is accomplished through the magnetic dipole interaction, which falls off with distance as r^{-3}. We have

used both the so-called second moment M_2 of the dipole interaction and two-dimensional experiments, which are explicitly sensitive to the dipole interaction itself, to estimate distances.

The second moment arises from a series expansion of the effect of the dipole coupling on the resonance line shape [39, 40]. It can be evaluated exactly, although it arises from a macroscopic number of coupled spins, because it depends on traces of the spin operators which can be evaluated in any basis and not necessarily the eigenbasis. The second moment takes the form

$$M_2 = E_L \gamma^4 \hbar^2 \sum_j \left(\frac{3}{2} \frac{1 - 3\cos^2 \theta_{ij}}{r_{ij}^3} \right)^2, \tag{4}$$

where γ is the gyromagnetic ratio, θ_{ij} is the angle between internuclear vector $\mathbf{r}_j - \mathbf{r}_i$ and the external field direction, and r_{ij} is the internuclear separation. E_L is a spin-dependent constant that includes matrix element effects that depend on which transitions are being excited [41]. The second moment can be measured from spin echoes [42, 43], because the normalized echo intensity decays as

$$\frac{I(\tau)}{I(0)} = 1 - \frac{M_2}{2!}\tau^2 + \frac{M_4}{4!}\tau^4 \ldots; \tag{5}$$

so, at short refocusing times τ, the decay is linear in τ^2 with slope $-M_2/2$. Elements of the material structure are encoded in M_2, which can be seen most clearly by recognizing that the sum over r_{ij}^{-6} in equation (4) can be replaced with an integral over the radial distribution function, since that function yields the number of particles found at a given distance r from a test particle at the origin [44]. Therefore we have

$$\sum_j \frac{1}{r_{ij}^6} \to \int \frac{4\pi \rho_0 g(r) r^2}{r^6} \mathrm{d}r, \tag{6}$$

where ρ_0 is the bulk number density of the species in question and $g(r)$ is the pair distribution function of that species. With this formalism measurements of M_2 can be quickly compared with models of the glass structure as expressed through their $g(r)$ functions. The experiment is carried out on a static sample, and so site selectivity is not particularly good.

More direct measurements of distance are obtained through two-dimensional NMR experiments that include explicit sensitivity to the dipole coupling. We have used the radio-frequency dipole recoupling (RFDR) method to study glass structure [45–47]. This experiment is carried out under MAS conditions; so good site selectivity is achieved. Since the dipole interaction is a rank-2 interaction, it is removed by MAS; the RFDR method re-introduces it, by applying a train of π pulses during a mixing time, which are synchronized with the rotor frequency. The result is a correlation between the indirect dimension, which is an MAS spectrum, and the direct dimension, also an MAS spectrum, with the correlation generated by dipole coupling during the intermediate mixing time. Cross-peaks are thus obtained which show magnetization that originated on one site during the indirect dimension, transferred to a second site during mixing time, and finally detected there during the direct dimension. Because of the r^{-3} dependence, only physically close sites can exchange magnetization in this way, resulting in a map of proximity of different types of site. This is quite powerful but is unfortunately difficult to interpret quantitatively. The dynamics of magnetization

exchange depend on the distance, as noted, but also on the chemical shift difference between the sites and the relative orientation of the chemical shift tensors between the sites [47, 48]. This last complication is serious, because obtaining the shift tensor orientations with respect to a molecular frame of reference is a time-consuming task usually necessitating single crystals. While this dependence is not strong enough to invalidate RFDR, it does render it better as a qualitative, rather than quantitative, probe.

2.2. *Neutron diffraction*

Because of the diverse length scales of importance in glass structure, the use of complementary structural probes provides a much more detailed picture of the structure than any one experiment alone can provide. Neutron diffraction is particularly convenient as a scattering probe of disordered materials and, because of its sensitivity to longer-range correlations, nicely complements NMR data [49].

The neutron data that we shall discuss was acquired on the glass, liquids and amorphous diffractometer (GLAD) at the intense pulsed neutron source (IPNS) at Argonne National Laboratory [50]. IPNS is a spallation neutron source, which provides pulses of neutrons with a substantial spread of energy. The GLAD instrument is a time-of-flight diffractometer, in which an array of helium detectors measure the diffracted neutrons, recording both the scattering angle 2θ and the flight time of each event. The flight time and path length are combined to determine the wavelength λ of each scattered neutron, and this information plus the scattering angle gives the momentum transfer through $Q = (4\pi \sin\theta)/\lambda$. Because of the range of energies and angles covered by the detectors, a wide range of Q values can be collected simultaneously, improving efficiency. Moreover, the instrument has been designed to optimize the Q range, while maintaining satisfactory resolution; good statistics out to $Q = 40$ Å^{-1} are achievable.

The experiment yields the total structure factor $S(Q)$, which, using the Faber–Ziman formalism, is composed of partial structure factors weighted by both the concentrations c_i and coherent scattering lengths $\bar{b}_i$ as

$$S(Q) = \sum_{i,j} W_{i,j} S_{i,j}(Q), \tag{7}$$

where

$$W_{i,j} = \bar{b}_i c_i \bar{b}_j c_j \Big/ \left(\sum_i \bar{b}_i c_i \right)^2. \tag{8}$$

Thus the measured $S(Q)$ contains a considerable amount of information, combining as it does the $n(n+1)/2$ distinct correlations between the n types of atom in the sample.

Presentation of the data as $S(Q)$ is helpful to assess longer-range correlations, which appear as features at low Q [2]; the short-range structure is easier to study in real space, that is from the total pair distribution function $G(r)$. This function is obtained from $S(Q)$ as

$$G(r) = \rho_0 + \frac{1}{2\pi^2 r} \int_0^{Q_{max}} Q[S(Q) - 1] \sin(Qr)\, \mathrm{d}Q, \tag{9}$$

where ρ_0 is the bulk number density and Q_{max} is the maximum Q value obtained in the experiment. This latter cut-off gives rise to truncation artefacts which complicate the analysis of the real-space data. We now turn to alternative means of analysing the information in $S(Q)$.

2.3. *Reverse Monte Carlo modelling*

To model the glass structure in a way consistent with our experiments we use the reverse Monte Carlo (RMC) method, due to McGreevy and colleagues [51, 52] and Wicks [12]. In this technique, a model of a material is constructed without the use of interatomic potentials. To optimize the model, atoms in it are moved at random and, at each stage, the structure factors, the pair distribution functions, or both are calculated and compared with experiment. If agreement with experiment is improved, in the least-squares sense, the move is accepted while, if agreement is not improved, the move is accepted with a probability dependent upon the uncertainty in the data sets. In this way, structures are generated that are consistent with experimental data. The limitations of this method arise primarily from the limited and possibly noisy data sets used to perform the optimization. For example, a three-component material is described by six partial structure factors, but almost never are six independent measurements available. Then the RMC optimizations must be done on a limited data set, and it has been found that structures consistent with the given data but inconsistent with reasonable chemical principles are easily generated. Additional constraints in the forms of nearest-neighbour cut-offs and coordination numbers are then added to the RMC calculation to account for this additional information. Particular care must then be exercised to avoid undue bias in the resulting structure. While the procedure can (and has) been criticized on the basis of requiring these additional constraints, it is our opinion that this feature is actually identical with more traditional methods of analysis, in which distances are extracted from real-space scattering data and then assigned on the basis of which bond lengths would be chemically reasonable. RMC merely automates this process and pinpoints errors much more vividly. RMC has also made vivid the *lack* of information in a total structure factor, given that excellent visual fits can be obtained for models that are not chemically reasonable. This again argues for building chemical insight into both the starting configuration of a model and the constraints under which it is optimized.

The need for extensive data sets presents an experimental challenge, which has been met admirably by several groups combining neutron diffraction with wide-angle X-ray scattering and extended X-ray absorption fine structure (EXAFS) [11, 12, 53–55]. We shall present a different approach to this problem, in which we combine neutron diffraction data with NMR results, in the form of coordination numbers and distances from second-moment measurements, to generate models consistent with all available data.

Having outlined the methods used for study, we now turn to specific examples of their applications.

3. Boron oxide glass and its modification

B_2O_3 is an important additive to commercial glasses, in part because it has the unusual property of raising the glass transition temperature, even in the presence of modifiers. This occurs because the threefold-coordinated boron in B_2O_3 is converted to fourfold-coordinated BO_4^- species, thereby increasing the average network coordination. This glass system has been studied by many techniques [56–61], and was the first to be examined using NMR [62]. It is an interesting system from a fundamental point of view, because the crystalline form of B_2O_3 cannot be made under ambient pressure conditions [63]. Thus one can study glass formation over a very wide range of preparation conditions. Also intriguing is the presence of boroxol rings, B_3O_3, linked

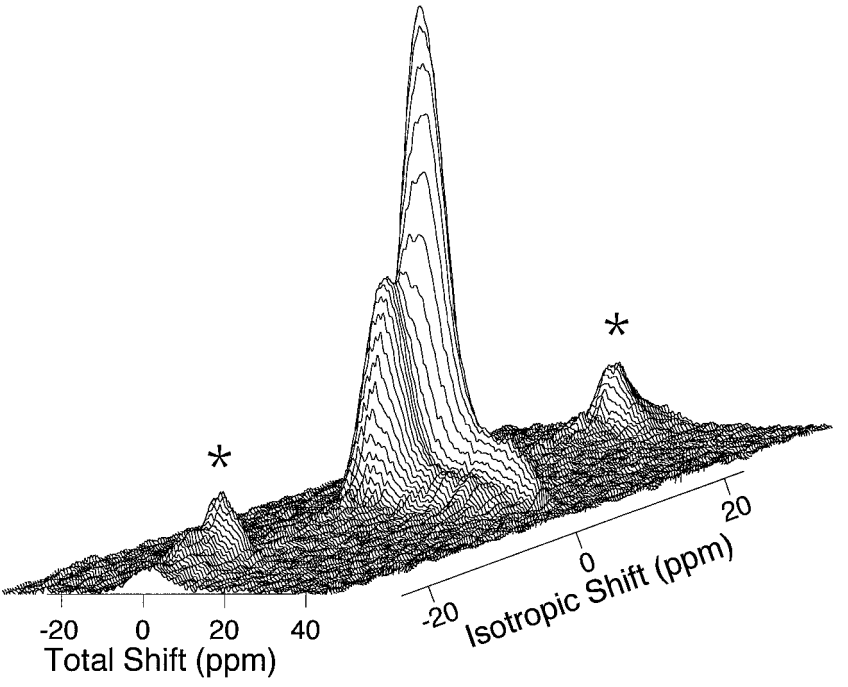

Figure 1. ^{11}B DAS NMR spectrum of B_2O_3 glass, showing resolution of two distinct boron sites: (*), spinning side bands. The stronger is assigned to boroxol rings, and the weaker to BO_3 units not in rings. The relative intensities are 0.7:0.3.

in the structure, which would constitute quite well defined intermediate-range order. As we shall discuss, the concentration of these units is a point of controversy in this material.

Here we review NMR studies of borate glasses, focusing on the issues listed above: intermediate range order in pure B_2O_3, and modification of the sites.

3.1. *Boron and oxygen sites from nuclear magnetic resonance*

Figure 1 shows the ^{11}B DAS NMR spectrum of B_2O_3 glass [60]. This spectrum shows two partially overlapping resonances, with intensity ratio of about 0.7:0.3. The two resonances have isotropic shifts of 4.7 ppm and 1.0 ppm at 8.4 T respectively; these shifts are the sum of the isotropic chemical shift and the second-order quadrupole shift (equation (3)). The contributions can be separated by performing the experiment at a different field; we have done this and find the parameters given in table 1. On the basis of the intensities (0.7 and 0.3) we assigned the down-field resonance to boroxol ring boron, and the up-field resonance to non-ring BO_3 units, in agreement with earlier work which suggested that between 60% and 80% of the boron are in boroxol rings. The chemical shifts as assigned in table 1 are in agreement with *ab initio* results of Tossell [64].

In alkali-oxide-modified glasses, as we shall discuss in more detail below, resonances with isotropic shifts of 4.7 ppm and 1.0 ppm are again observed at 8.4 T, with a third resonance at -0.3 ppm appearing as the alkali oxide concentration is increased. Here we wish to discuss the results obtained from the NMR spectra of potassium borate crystals [65]. The crystal structures of the compounds studied are all known, and so the boron resonances can be assigned unambiguously from their

Table 1. Parameters of ^{11}B Resonances in B_2O_3 glass at 8.4 T magnetic field: relative populations, total isotropic shifts, isotropic chemical shifts and quadrupole products. Shifts are relative to $BF_3 \cdot Et_2O$. The quadrupole product is given by $P_Q = (e^2Qq/h)(1+\eta^2/3)^{1/2}$, with e^2Qq/h the quadrupole coupling and η the quadrupole asymmetry.

Population	δ_{iso} (ppm)	δ_{CS} (ppm)	P_Q (MHz)
0.7	4.7	18.0	2.7
0.3	1.0	13.0	2.6

Table 2. Isotropic shifts of boron in various structural units found in borate crystals, at 8.4 T relative to $BF_3 \cdot Et_2O$.

Structural unit	Isotropic shift (ppm)
Non-ring BO_3	1.0–2.3
BO_4^-	− 0.3
BO_3: metaborate	4.9
BO_3: pentaborate	3.7
BO_3: triborate	3.8
BO_3: di-triborate	5.4
BO_3: diborate	5.4

intensities. The assignments are shown in table 2. The first point to note is that boron in the metaborate ring, $B_3O_6^{3-}$, has an isotropic shift of 4.9 ppm, almost identical with the 4.7 ppm shift seen in the glass. The metaborate ring is a planar boroxol ring capped by a NBO atom. Next, in the crystals, non-ring BO_3 groups are found in the range 1.0–2.3 ppm, with the down-field shift arising from a BO_3 group with two BO_4^- neighbours. BO_3 groups in modified boroxol rings have isotropic shifts within a part per million of the metaborate shift, never farther upfield than 3.8 ppm. These results on crystalline compounds are, in our opinion, only consistent with assignment of the 4.7 ppm shift in the glass to boroxol rings, and the 1.0 ppm shift to non-ring BO_3 groups. This assignment leads to 70% of the boron in boroxol rings, and to 30% in non-ring units, in agreement with numerous previous estimates [59, 66, 67]. On the other hand, it must be noted that several computational studies of glassy B_2O_3 structure find only a small fraction of rings, essentially what would be present through statistical linkages alone [68, 69]. It is not clear that these models yield two distinct boron sites, of the type observed in the NMR and nuclear quadrupole resonance experiments [58, 60], and so they are difficult to reconcile with the present data.

The different borate units are linked through oxygen, and using the DOR experiment we were able to resolve three different oxygen sites, with relative intensities of 0.5:0.3:0.2 [61]. The shifts and quadrupole parameters indicate that all three sites are bridging oxygen. To assign these sites we constructed a model based on the assumption that four resolvable oxygen sites could be present: oxygen in boroxol rings, oxygen bridging boroxol rings, oxygen bridging rings and non-ring BO_3, and finally oxygen bridging two non-ring BO_3 units. Two facts were used to constrain the concentrations of these four units: the ratio of oxygen to boron in the glass (3:2) and the fraction of boron present in rings (0.7, based on our NMR data on these samples). This is sufficient to constrain the oxygen site populations leaving only a single degree

of freedom. For example, consider the ring oxygen. Call the number of ring boron atoms R; then there are also R ring oxygen atoms, since the ring composition is B_3O_3. The fraction of ring oxygen is then R/N, where N is the total number of oxygen atoms, but $N/M = 3/2$, where M is the total number of boron atoms. Therefore $R/N = 2R/3M = 0.7 \times 2/3 = 0.47$, since for the fraction of boron in rings $R/M = 0.7$. We thus assign the experimentally observed resonance with intensity 0.5 as the ring oxygen site (note that there are no adjustable parameters in this assignment). For the other three oxygen sites, two independent equations may be derived, following reasoning similar to the above. The solutions of these equations may be found in terms of one of the three unknowns, and they show that there is only one region of solution space that corresponds to the observed intensities of 0.5, 0.3 and 0.2, namely when the population of ring to non-ring bridging oxygen is small.

A small concentration of ring to non-ring connections suggests that the glass consists of regions rich in boroxol rings, and regions poor in rings. From the size of rings and the assumption that each ring on the surface of a ring-rich region makes a single connection to non-ring BO_3 units, we estimated the size of the ring-rich regions to be about 20–40 Å. Interestingly, recent light-scattering measurements at the glass transitions in B_2O_3 are consistent with structural inhomogeneities on this length scale [3, 70]. Indeed, intermediate-range order is conjectured to be universal in glass formation. Our data suggests its structural origin in this particular material.

3.2. *How the sites are modified*

Because of the presence of both boroxol rings and non-ring BO_3 units in the pure glass and melt [71] the modification to BO_4^- could happen at either site or both. Considerable work using Raman spectroscopy indicates that the pure boroxol rings are modified in some way, as the sharp 808 cm^{-1} peak indicative of the boroxol rings diminishes in intensity and is replaced by a broader feature at about 770 cm^{-1}.

Figure 2 shows ^{11}B spectra of K_2O-modified borate glasses, which also provide a way to follow the structural changes upon modification. In this figure it is clear that, as more modifier is added, the less intense peak at 1.0 ppm decreases in intensity, while a new feature grows at -0.3 ppm. The strong feature at 4.7 ppm decreases slightly. These three resonances are all well fitted by Gaussian line shapes, and from such fits the relative intensities of the three resonances can be extracted.

At 0% modifier (pure B_2O_3 glass) the features in the NMR spectra are due to boroxol ring boron (4.7 ppm) and non-ring BO_3 units (1.0 ppm). The feature at -0.3 ppm is due to four-coordinated boron (table 2). As noted above, Raman spectra strongly indicate that the symmetric boroxol ring is modified, presumably being converted to triborate (two threefold- and one fourfold-coordinated boron in a ring) and more complex ring structures. DAS NMR also indicates that substantial modification occurs at the non-ring BO_3 sites, which decrease markedly in intensity as modifier is added [65, 72].

We constructed a model of the modification by using the NMR data to quantify the loss of loose BO_3 units and the gain of BO_4^- units (of all types), and the Raman data to quantify the loss of boroxol rings [65]. The NMR data show only a slight loss of intensity at the 4.7 ppm peak, as a function of modifier; recall that this peak is due to boroxol rings in pure B_2O_3 glass. However (table 2), we found that BO_3 groups in all sorts of rings have a shift of about 4.7 ppm, whether in boroxol rings or in modified rings. Thus the 4.7 ppm peak quantifies the fraction of threefold-coordinated boron in rings of all types. The resulting model fits both the NMR and the Raman data. It

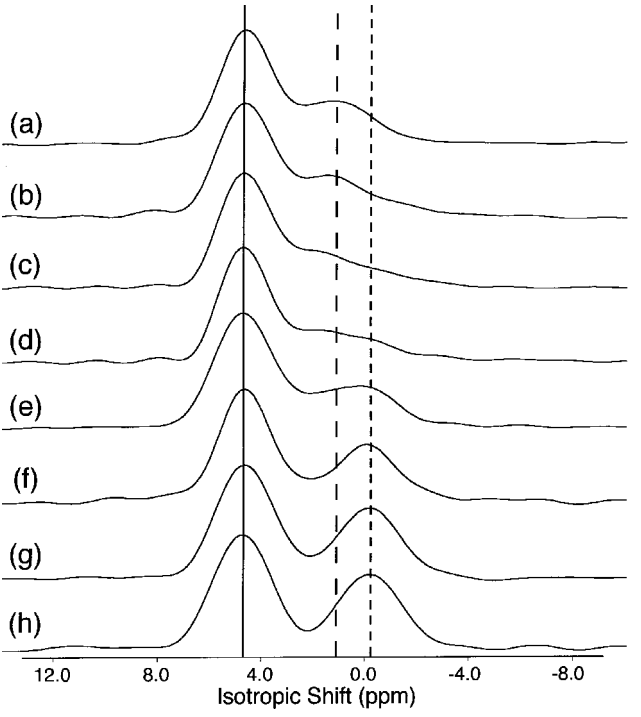

Figure 2. ^{11}B DAS spectra of potassium borate glass, as a function of added modifier. Note the loss of intensity at 1.0 ppm and gain at −0.3 ppm; the latter site is due to four-coordinated boron. The amounts of added potassium oxide (K_2O) are as follows: (*a*) 0 mol% ; (*b*) 8 mol% ; (*c*) 13 mol% ; (*d*) 18 mol% ; (*e*) 23 mol% ; (*f*) 28 mol% ; (*g*) 33 mol% ; (*h*) 38 mol%.

makes two particularly interesting predictions: first, that the non-ring BO_3 sites are modified at a somewhat higher rate than the boroxol ring boron and, secondly, that, once a loose BO_3 site has been modified, there is a propensity for neighbouring sites to close around it, making an additional modified ring. Both predictions suggest that rings are particularly stabilizing features in this system.

4. Silver iodide–silver phosphate: a superionic conductor

AgI–$AgPO_3$ glasses are intriguing examples of fast-ion conductors. These systems contain P_2O_5 as network former and Ag_2O as network modifier and undergo typical modification chemistry. Addition of the modifier M_2O cleaves the network, creating NBO atoms, charge compensated by M^+ cations. Glasses consisting of only Ag_2O and P_2O_5 do not show particularly remarkable conductivity properties. Inclusion of the salt AgI, however, is accompanied by orders-of-magnitude increases in ionic conductivity, while the electronic conductivity remains low. In glasses with over 50% AgI, the conductivity is comparable with those of dilute aqueous salt solutions, while the material as a whole remains a hard brittle solid. Good ion conductors such as this are attractive candidates for electrochemical applications such as batteries, sensors and fuel cells, and the possibility of making all-solid-state or even all-glass batteries is appealing, because of their potential ease of fabrication and resistance against leakage.

The mechanism of ion motion in glassy fast-ion conductors remains unclear, despite considerable research. In particular, the connection between the glass structure

and ionic mobility has been difficult to discover but is especially interesting given the orders of magnitude difference in time scale of the ion dynamics as against structural dynamics that develops below the grass transition temperature. An early conjecture was that the added AgI is somehow stabilized into the α-AgI phase, a known fast-ion conducting crystal that is stable above 147 °C. Evidence for this came from the conductivity of the glasses as a function of added AgI, which appeared to extrapolate towards the conductivity of pure α-AgI, and several X-ray scattering measurements. Recent diffraction measurements and modelling have suggested that, in contrast, the added AgI does not form clusters but in fact dissolves essentially homogeneously into the glass, functioning instead to open up the structure of the material.

In the following we shall discuss studies that we have made with NMR on $AgI–AgPO_3$ glasses, directed both at probing the silver dynamics and at investigating changes in the phosphate network.

4.1. ^{109}*Ag nuclear magnetic resonance: a probe of cation binding and dynamics*

While ^{7}Li, a relatively convenient NMR nucleus, has been used extensively to study lithium conducting materials, ^{109}Ag, which is a rather difficult NMR nucleus, has been used only rarely to study silver conductors [73–75]. The difficulties include low frequency (16.7 MHz at 8.46 T), large chemical shift range and long relaxation times. Nonetheless the large chemical shift range provides a good opportunity, because of the sensitive structural discrimination it affords.

We found that the chemical shift of ^{109}Ag in $AgI–AgPO_3$ glasses varies strongly with added AgI [75]. Because of the high conductivities in these glasses, even at the 10% AgI level a motionally narrowed ^{109}Ag spectrum is obtained, and line-narrowing techniques such as MAS are unnecessary. The chemical shift as a function of AgI shows a nonlinear dependence reminiscent of silver in ethylamine–halide solutions [76]. This indicates that the silver is coordinated to both oxygen and iodine over the course of the experiment. Moreover, the nonlinear shift behaviour as a function of AgI indicates that the effects are not merely additive, which argues against the presence of separated AgI and $AgPO_3$ domains in the material. Our conclusion from this experiment is that AgI dissolves homogeneously into the glass, and the silver cations interact with both oxide and iodide anions.

The dynamics of the silver cations can be probed through variable-temperature experiments. The silver resonance narrows appreciably as temperature is increased, as expected. Most significantly, at low temperatures where motion has slowed below the NMR timescale, even MAS did not resolve more than a single broadened site,. This is strong evidence for structural homogeneity of the silver sites and again argues against AgI domains within the phosphate matrix. It also suggests that a strong electrolyte picture is most appropriate for this glass electrolyte, as all cations appear to be mobile, and the conductivity is determined principally by their mobility (as opposed to concentration).

4.2. ^{31}*P nuclear magnetic resonance studies of the phosphate network*

As noted in section 2.1.2, the RFDR experiment provides a convenient qualitative probe of distances in a glass. We have used this experiment to probe the structural effect of added AgI in $AgPO_3$ glasses, and the results are shown in figures 3 and 4. Figure 3 shows the two-dimensional ^{31}P spectra of glassy $AgPO_3$ and $(AgI)_{40}(AgPO_3)_{60}$. The chemistry suggests, and MAS experiments confirm, that these glasses consist of only a single type of phosphate site, which has two bridging and two

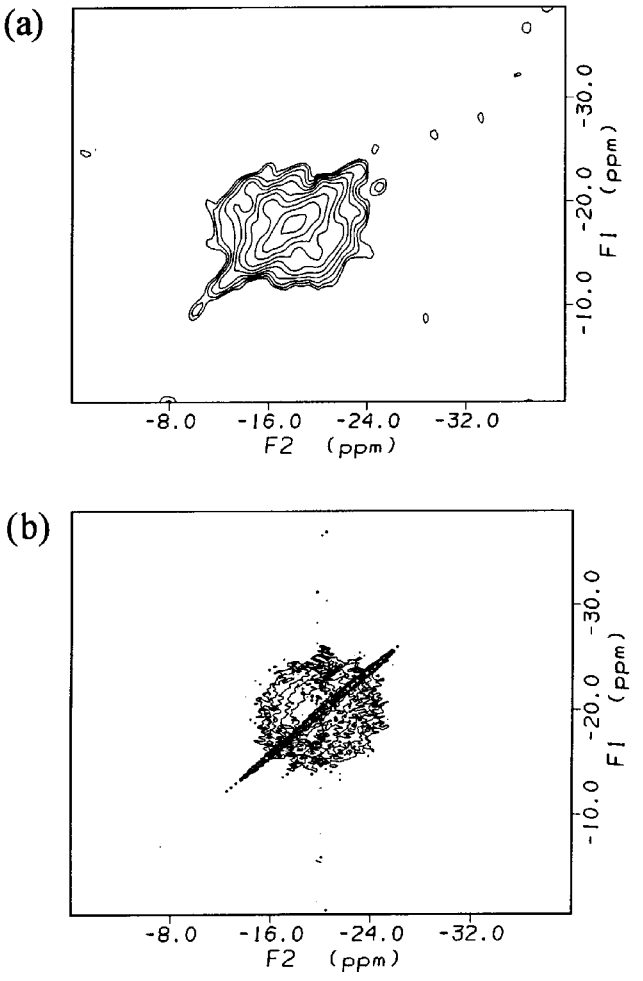

Figure 3. RFDR ^{31}P spectra of AgI–$AgPO_3$ glasses: (*a*) glassy $AgPO_3$; (*b*) $(AgI)_{40}(AgPO_3)_{60}$. Both are shown at a mixing time of 12.6 ms. The single site in each is due to phosphate with two bridging oxygen and two NBO ligands, the only type of phosphorus in these glasses.

NBO ligands. The result is a structure consisting of long phosphate chains, or possibly rings. Diffraction measurements do not indicate the presence of small rings; large rings are probably indistinguishable from long chains. The RFDR data show a single phosphate site, with exchange intensity that spreads into the two-dimensional plane during the mixing time of the experiment. Physically, this represents magnetization that transferred from one chemically equivalent but physically distinct site to another during the portion of the experiment in which dipole coupling is reintroduced. Interestingly, at equal mixing times, figure 3 shows that the sample with 40% AgI retains a non-exchanged component, while the sample without AgI shows complete exchange at the same mixing time. The difference between exchanged and non-exchanged magnetization is shown graphically in figure 4. This surprising result is consistent with models of this glass, which predict that the structural effect of AgI is in part to spread the phosphate chains apart. Our results indicate that, as AgI is added, magnetization is increasingly trapped and does not exchange as readily, in part we

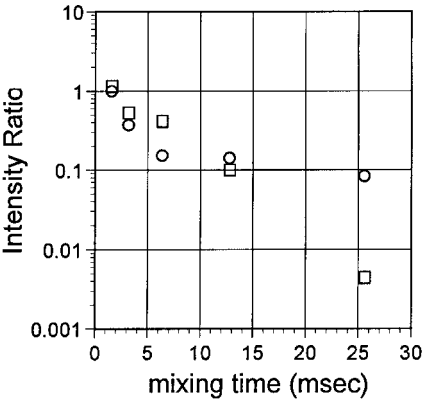

Figure 4. Ratio of non-exchanged to exchanged magnetization for $AgPO_3$ (□) and $(AgI)_{40}(AgPO_3)_{60}$ (○), as a function of mixing time. Note the exponential decrease for $AgPO_3$, and the plateau for $(AgI)_{40}(AgPO_3)_{60}$, indicating a significant fraction of very slowly exchanging magnetization.

believe because there are fewer near neighbours with which to exchange. While the number of nearest neighbours stays fixed at two, owing to the phosphate chain structure it must be remembered that the r^{-3} form of the interaction is long range, in the sense that $\int r^2 \, dr/r^3$ diverges logarithmically. Therefore, more distant spins are as significant as nearby spins, and the experiment probes the net loss of neighbours over extended length scales, and not just short range. Thus the NMR results give direct confirmation of the models constructed on the basis of diffraction data [12].

5. Tellurites: nuclear magnetic resonance, crystallography and neutron diffraction

The third system that we shall discuss is tellurite-based glass, that is glass in which TeO_2 is the glass network former. Because of the lone electron pair on each tellurium atom, the nonlinear optical susceptibility of these glasses is quite high [77, 78]. This feature, coupled with the good solubility of rare-earth ions in tellurites, has generated interest in this system as a potential optical switching material and laser host. Fundamentally, it is intriguing that TeO_2 itself is only a marginally good glass former, in contrast with other four-coordinated oxides such as silica (SiO_2). Modified tellurites, on the other hand, typically show a broad range of good glass formation [79–81]. Here we shall be concerned with alkali oxide-modified tellurites, of the form $(M_2O)_x(TeO_2)_{1-x}$, with M an alkali metal. Heo *et al.* [80] showed that, in this system, sodium tellurite is particularly stable, especially at the $x = 0.20$ composition. Here stability is meant in the sense of warming the glass above the glass transition temperature while still avoiding crystallization. Their data is summarized in figure 5. Most intriguingly, the composition of the reported stability maximum coincides with one of the crystal phases in this system, $Na_2Te_4O_9$.

Earlier studies of tellurite glass structure focused primarily on changes in the tellurite matrix upon modification [79, 80, 82–85]. Pure tellurite (TeO_2) is a fully linked network of $TeO_{4/2}$ trigonal bipyramids (the lone pair occupying one of the equatorial sites) [86], while alkali tellurite (M_2TeO_3) is an ionic solid consisting of TeO_3^{2-} anions [87]. The glass-forming range lies between these extremes, and it is important to discover how the network responds to intermediate levels of modifier. Unfortunately, there were significant gaps in the knowledge of the crystal chemistry of tellurites in this range [88]. Without crystal data for comparison it is particularly difficult to interpret

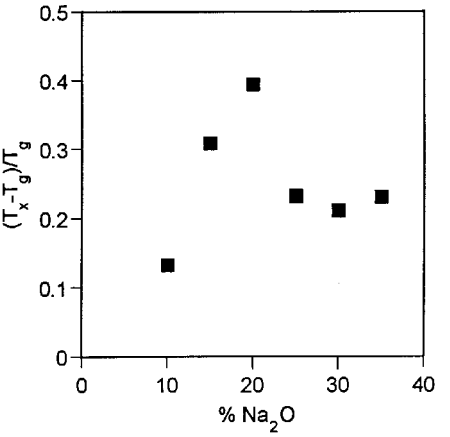

Figure 5. Difference between crystallization temperature T_x upon heating and glass transition temperature, T_g, scaled to T_g for $(Na_2O)_x(TeO_2)_{1-x}$ glasses as a function of added sodium oxide (Na_2O). The peak at 20 mol% suggests that this composition is particularly stable against devitrification. (Data taken from [80].)

data on such a complex glass. To approach this problem we have combined three techniques: crystallography to fill in the gaps in the solid-state chemistry of the crystal phases, NMR to measure the environments of the modifying ions, and neutron diffraction to probe changes in the tellurite network. The results of these studies are combined in a consistent way using RMC modelling, to generate models of the glass structure consistent with the available experimental data.

5.1. *Bonding in the tellurites*

The solid-state chemistry of the tellurites is somewhat more complex than, for example, silicates. While the tellurium atoms remain as Te^{IV}, their coordination numbers change, and the formal charge on the anions change, as modifiers are added. In silicate glasses, in contrast, silicon remains fourfold coordinated as modifiers such as alkali oxides are added; the primary change in the short-range structure is that bridging oxygen bonds are cleaved as the newly introduced oxygen are incorporated into the network, resulting in NBO with formal charge of -1. In tellurites, on the other hand, the structure of the unmodified material consists of $TeO_{4/2}$ units, with four bridging bonds in a three-dimensional network, while the M_2TeO_3 composition (that is 50% added modifier M_2O, with M an alkali metal) consists of M^+ cations coordinated by TeO_3^{2-} anions. In the TeO_3^{2-} anion the formal charge is obviously -2, while there are three NBO atoms and the oxidation number of tellurium is still four. The charges on the oxygen are delocalized across several centres, owing to the participation of d orbitals in the basic bonding scheme. In fact, d bonding is significant already in unmodified TeO_2 because, in addition to the four bonds in which each tellurium atom participates, each must also accommodate a lone pair of electrons. The lone pair provides added richness to the chemistry and also confers utility on tellurite glasses in the form of high nonlinear optical susceptibilities, compared with more traditional oxide glasses.

Between the unmodified TeO_2 and fully modified M_2TeO_3 lies the glass-forming compositions of the tellurites, which, depending on the particular alkali modifier M in use, occur in roughly the 5–30 mol% range [80]. In this range lies two more crystal phases: $M_2Te_4O_9$ (20% modifier) and $M_2Te_2O_5$ (33% modifier) [88]. Crystal

structures for some of these phases were known, but not the potassium versions, and in particular not the key sodium compounds. We were able to grow single crystals of $M_2Te_4O_9$ and $M_2Te_2O_5$, both with M = Na and with M = K [89–91]. In addition to providing important reference data on the tellurite structures, with which the glasses may be compared, these results give us the opportunity to identify structural trends in the tellurites, as the cation size is changed. Our key conclusions in this regard are two. First, we found that the number of NBO atoms at a given composition depends markedly on the identity of the modifying cation. This result is not at all expected on the basis of the simple picture of modifiers acting simply to cleave bridging bonds, leaving NBO atoms behind. In fact, we found that, in the tellurites, larger ions induce a higher number of NBO atoms, at the 20% and 33% compositions; at the 50% composition, the ratio of NBO atoms to modifying ions is always 3:2. The numbers are summarized in table 3. A similar trend exists for the types of tellurite structure produced, which range from $TeO_{4/2}$ (four bridging oxygen atoms), in pure tellurite, to the TeO_3^{2-} anions of the 50% modified compounds, which have three NBO atoms and a total charge of −2. In between are found a variety of species, such as $TeO_{3/2}O^-$, with three bridging oxygen atoms and one NBO atom, and so forth. The trend again is that the large cations induce the more highly charged groups, with more NBO atoms per tellurium atom, more quickly. The data are summarized in table 4.

The explanation for this cation size dependence, we believe, arises from the bulkiness of the produced anions. The target structure in this system is the TeO_3^{2-} anion; all modification leads to this eventually. Along the way, however, intermediate structures are formed which must pack around the cations. In all these structures, the negative charge can be delocalized over several oxygen atoms. It seems reasonable that the larger structures will pack less efficiently around small cations, such as lithium, owing to Coulomb repulsion effects. This would explain why fewer NBO atoms are formed in the lithium compounds, since a high degree of NBO formation requires a high degree of charge delocalization, and hence large bulky tellurite anions. This Coulomb repulsion is less severe in the potassium and caesium cases, since the much larger cations provide more surrounding space in which to pack the tellurite anions. More charge delocalization is then possible, leading to more NBO formation.

5.2. *The distribution of modifiers*

While much attention in this field has focussed on changes in the network upon modification, we have just seen that the modifying ions themselves play a significant role, by dictating the structure of their surroundings. The alkali ion environment is difficult to probe in glasses; notable successes have been achieved using EXAFS [92–94]. We have used NMR to study the modifiers, in particular sodium in sodium tellurite glasses [44, 89, 95].

^{23}Na is a convenient NMR nucleus, which is 100% abundant, has spin $\frac{3}{2}$ and resonates at 95 MHz in an 8.4 T magnet (in which protons resonate at 360 MHz). Because of the quadrupole moment and small chemical shift range, little direct information is obtainable using conventional solid-state NMR techniques such as MAS. Using DAS and comparing the results from several magnetic fields, however, we could obtain good results on the average environment that the sodium cations occupy as a function of modifier content [89, 95]. In contrast with applications of DAS to borates, discussed in section 3, the goal here was not to resolve similar sites, but rather to measure the average isotropic shift parameters. In these glasses there are not distinct classes of cation sites, rather there is a broad distribution of sites. Under

Table 3. Cation and NBO in alkali tellurite crystals. Listed for each composition are the coordination numbers CN of oxygen around the crystallographically distinct alkali cation sites, and the number of NBO atoms per oxygen, alkali cation and tellurium atom per formula unit. Note the strong cation size dependence, particularly in the number of NBO atoms per alkali cation.

Modifier (mol%)	Composition	M^+ CN	NBO per O	NBO per M^+	NBO per Te
0	α-TeO_2	—	0	—	0
	β-TeO_2	—	0	—	0
20	$Na_2Te_4O_9$	4, 5	0.22	1.0	0.5
	$K_2Te_4O_9$	6, 7	0.44	2.0	1.0
	$Cs_2Te_4O_9$	6, 7	0.44	2.0	1.0
33	α-$Li_2Te_2O_5$	3, 4	0.4	1.0	1.0
	β-$Li_2Te_2O_5$	3, 4	0.4	1.0	1.0
	$Na_4Te_4O_{10}$	5, 6	0.6	1.5	1.5
	$K_2Te_2O_5$	7, 7	0.6	1.5	1.5
	$Cs_2Te_2O_5$	6, 9	0.8	2.0	2.0
50	Li_2TeO_3	4, 4	1.0	1.5	3.0
	Na_2TeO_3	6, 6	1.0	1.5	3.0
	K_2TeO_3	6, 6, 6	1.0	1.5	3.0
	Cs_2TeO_3	6, 6, 6	1.0	1.5	3.0

Table 4. Tellurite structures found in different alkali tellurite crystals.

Modifier (mol%)	Composition	$TeO_{4/2}$	$Te_{3/2}O^-$	$TeO_{2/2}$	$TeO_{1/2}O_2^-$	TeO_3^{2-}
0	α-TeO_2	1				
	β-TeO_2	1				
20	$Na_2Te_4O_9$	1	2	1		
	$K_2Te_4O_9$		2	2		
	$Cs_2Te_4O_9$		2	2		
33	α-$Li_2Te_2O_5$		2			
	β-$Li_2Te_2O_5$		2			
	$Na_4Te_4O_{10}$		1		1	
	$K_2Te_2O_5$		1		1	
	$Cs_2Te_2O_5$				2	
50	Li_2TeO_3					1
	Na_2TeO_3					1
	K_2TeO_3					1
	Cs_2TeO_3					1

conventional MAS, however, this distribution is broadened additionally by the anisotropic portions of the chemical shift and quadrupole interactions. With DAS we could measure the pure isotropic shift pattern, still broadened by disorder but with no contribution from anisotropy. This shift, as noted above, includes both the chemical shift and the second-order quadrupole effects, which we disentangled by acquiring the data at two different magnetic field strengths.

The quadrupole parameter, shown in figure 6, reflects primarily the local symmetry of the oxygen shell that coordinates the sodium cation. For ionic interactions such as

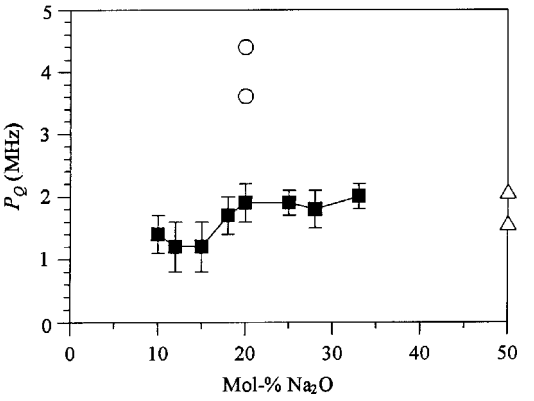

Figure 6. Quadrupole product $P_Q = (e^2Qq/h)(1+\eta^2/3)^{1/2}$ for sodium in $(Na_2O)_x(TeO_2)_{1-x}$ glasses as a function of added Na_2O. Here e^2Qq/h is the strength of the quadrupole interaction, and η the asymmetry of the interaction. Local environments with tetrahedral or greater symmetry have $e^2Qq/h = 0$, so the increase in P_Q at least 20 mol% Na_2O suggests a *decrease* in local symmetry around the sodium cations. The open symbols show P_Q for crystals of the given compositions.

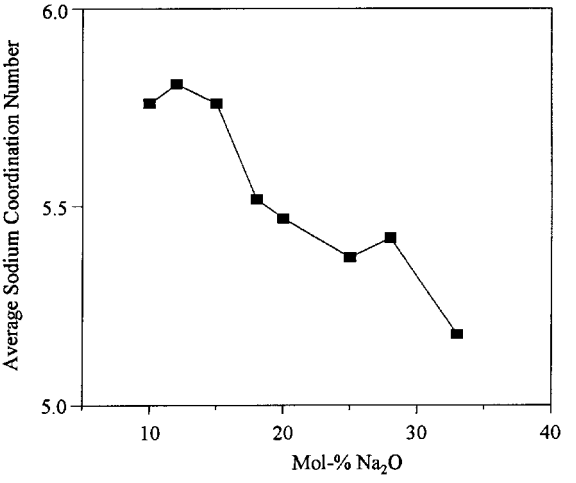

Figure 7. Estimated coordination number of oxygen around sodium in $(Na_2O)_x(TeO_2)_{1-x}$ glasses, as a function of added Na_2O. This estimation is based on the sodium chemical shift. Note the abrupt onset of decline near 20 mol% modifier.

these a point-charge model is adequate [96], and within this model it is clear that tetrahedral or greater symmetry gives zero quadrupole interaction. Figure 6 shows a low quadrupole interaction until the 20 mol% modifier concentration, at which point the interaction strength increases abruptly. This signals a decrease in the local symmetry around the cations. The interaction strength in the $Na_2Te_4O_9$ crystal, however, is substantially higher than in the glass, indicating that the sodium coordination shell in the crystal is significantly more strained (locally) than in the glass. This is not unreasonable, since the crystal must have lower total free energy, while the glass can have more relaxed local structure but higher overall free energy.

The chemical shift of alkali cations in oxides, and sodium in particular, depends on the number and proximity of the oxygen atoms that coordinate it [96, 97]. Therefore, from the sodium chemical shift as a function of composition, we could estimate the

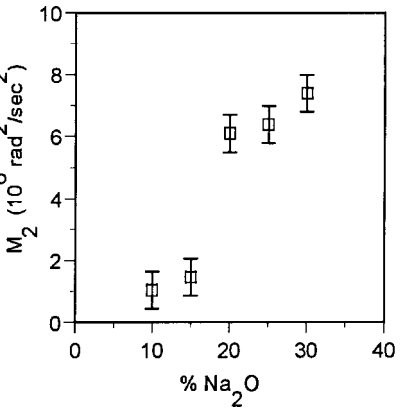

Figure 8. Magnetic-dipole weighted second moment of sodium distribution in $(Na_2O)_x(TeO_2)_{1-x}$ glass, as a function of added Na_2O. This quantity is derived from spin-echo measurements, and is related to the proximity of sodium cations. Note the sharp increase at 20 mol%.

sodium coordination number. The coordination number is plotted in figure 7 and shows, similarly to the quadrupole interaction data, an abrupt change near the 20 mol% modifier concentration. At low modifier content an average cation is coordinated by about 6 oxygen neighbours, but this number decreases roughly linearly with increasing modifier concentration at the 20 mol% level and above. We conjecture from these results that the local coordination shell is becoming dominated by NBO atoms, in accord with our findings from crystallography, which showed an increase in NBO content at higher modifier levels. The onset of coordination number decrease is fairly abrupt and, like the quadrupole interaction data, signals a substantial change in glass structure at this composition.

The proximity of modifying cations to each other is further evidence for significant structural change in the sodium tellurite system. We used spin-echo NMR measurements to determine this proximity [44]. In the absence of motion, spin echoes decay primarily owing to magnetic dipole coupling, an interaction that has an r^{-3} distance dependence. In sodium tellurites, there is negligible heteronuclear contributions to this decay, owing to the low abundance and low gyromagnetic ratio of NMR active isotopes of oxygen and tellurium. We could therefore use the methodology outlined in section 2.1.2 to measure the second moment M_2 of the sodium dipole distribution and to relate it to an integral over $g(r)$, the sodium pair distribution function. The M_2 data for sodium tellurite glasses is reproduced in figure 8. Note the monotonic increase with increasing sodium content; this is a trivial consequence of the increased sodium density, and hence closer proximity and increased M_2. More interesting is the sharp increase in M_2 at, again, the 20 mol% concentration, suggesting an abrupt decrease in typical Na–Na contact distances.

A full model of the glass structure must include not only the modifier ion environment but also the structure of the glass network. This is not easily accessible from NMR; so to probe it we use neutron diffraction. We turn to these studies now.

5.3. *Neutron diffraction and models of the glass*

The NMR measurements described above are particularly effective as probes of the local environment of the cations. The glass structure over longer length scales is studied more effectively using scattering experiments, and in particular neutron

Table 5. Faber–Ziman weighting factors for neutron diffraction in $(Na_2O)_x(TeO_2)_{1-x}$ glasses, as a function of Na_2O content.

Na_2O (mol%)	$W_{Te,\,Te}$	$W_{Te,\,O}$	$W_{Te,\,Na}$	$W_{O,\,O}$	$W_{O,\,Na}$	$W_{Na,\,Na}$
10	0.095	0.400	0.026	0.423	0.055	0.002
15	0.087	0.378	0.038	0.411	0.082	0.004
20	0.079	0.355	0.049	0.400	0.110	0.008
25	0.071	0.333	0.059	0.388	0.137	0.012
30	0.064	0.310	0.068	0.377	0.164	0.018

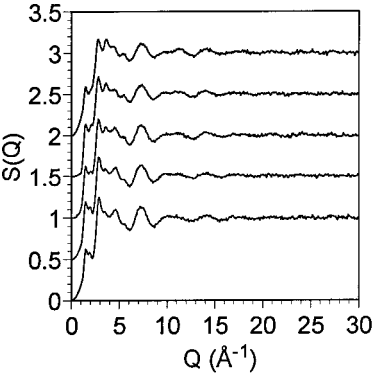

Figure 9. The total Faber–Ziman structure factor $S(Q)$ for $(Na_2O)_x(TeO_2)_{1-x}$ glass, obtained using neutron diffraction. The Na_2O contents, from bottom to top, are 12 mol%, 15 mol%, 20 mol%, 25 mol% and 28 mol%. The curves are offset by 0.5 units.

diffraction. We have made neutron diffraction measurements on a variety of alkali tellurites and here present some of our first results on $(Na_2O)_x(TeO_2)_{1-x}$ glasses.

Figure 9 shows the result of a neutron diffraction measurement on a glass, namely the function $S(Q)$. This function expresses the intensity of scattering by the sample at momentum transfer Q. The sine Fourier transform of $S(Q)$ is related to the pair distribution function, from which real-space information about the atomic co-ordination and bond lengths may be extracted. The problem is that each of these functions is comprised of partial distribution functions (equation (7) and (8)). In $(Na_2O)_x(TeO_2)_{1-x}$ there are six such partials, with weight factors as given in table 5. Note that Te–O and O–O correlations make the largest contributions to the structure factors, because of the high concentrations. The Te–Te contribution is less, and the contributions involving sodium are much less, owing to the low concentrations and smaller scattering length of sodium. Thus direct interpretation of the real space data associated with the total $S(Q)$ in this system yields information mainly about the Te–O and the O–O distances.

To build more complete models we have extended the RMC formalism outlined in section 2.3 to include not only fits to $S(Q)$ and/or $g(r)$ from scattering data, but also the results of NMR measurements on proximity of neighbouring nuclei. For $(Na_2O)_x(TeO_2)_{1-x}$ glasses this is relatively simple, because as we showed above (equation (6)) the second moment from NMR can be mapped onto an integral over the relevant pair distribution function. These pair distribution functions are calculated as a standard part of the RMC algorithm; so incorporation of M_2 as an additional constraint is simply a matter of calculating an additional integral. Table 5 indicates the

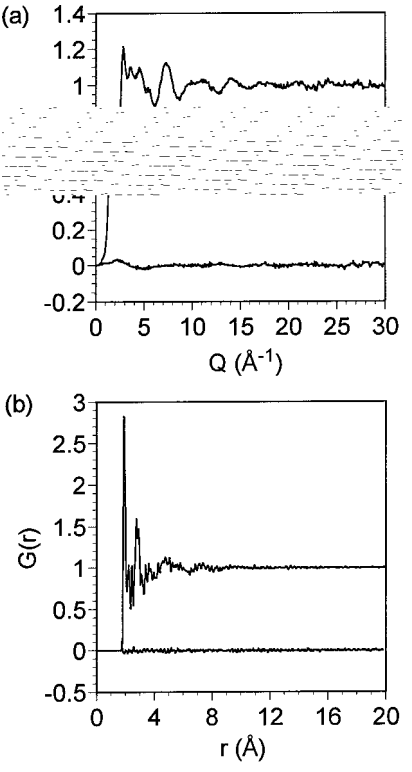

Figure 10. Data and RMC fits to (*a*) $S(Q)$ and (*b*) $G(r)$, with residuals, for $(Na_2O)_{20}(TeO)_{80}$ glass. The fits also incorporate constraints on the sodium coordination number and Na–Na proximity derived from NMR data.

advantage of this procedure; the contribution of sodium to the partials is always small, in both neutron scattering and X-ray scattering; so additional information is necessary to constrain the positions of the cations appropriately.

We are carrying out this procedure on models of $(Na_2O)_x(TeO_2)_{1-x}$ with 3750 atoms, which occupy a cubic sample cell of roughly 20 Å per side. The RMC procedure is run to fit to both $S(Q)$ and the total $g(r)$, the Na–O coordination number derived from the NMR experiments described above (figure 7), and the sodium M_2 values as derived from spin-echo measurements, also as described above (figure 8). Information from the crystallography that we have done was used to set the closest-approach distances of the different atom pairs. Figure 10 shows the fits to the data, with residuals.

The fits are visually excellent, but caution must always be exercised in interpreting these models since although we combined NMR with neutron diffraction, we are still short of a total data set constraining all six partials. Nonetheless, the coordination numbers, bond lengths and bond angles that the models predict agree reasonably with those obtained from crystallography, giving confidence that the RMC algorithm is yielding useful information.

From the RMC models we seek to discover how the structure changes with added modifier. Our first result is shown in figure 11, which shows the Na–Na pair distribution function as Na_2O is added to the glass. Figure 8 indicated that the second

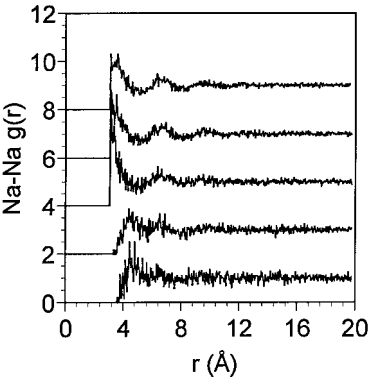

Figure 11. Na–Na partial pair distribution functions for $(Na_2O)_x(TeO_2)_{1-x}$ glass, derived from RMC models. Na_2O contents, from bottom to top, are 12 mol%, 15 mol%, 20 mol%, 25 mol% and 28 mol%. The curves are offset by 2 units.

moment of the sodium distribution increases markedly at 20 mol% ; here we see this effect in the full model. Recall that M_2 was used in constructing these models, but that there are many $g(r)$ values consistent with the same M_2. What is shown here is the $g(r)$ consistent with not only the measured M_2 value but also the neutron diffraction data (figure 9) and coordination constraints derived from NMR (figure 7). The $g(r)$ values at low modifier content are quite spread out, showing even less of an initial peak than would a hard-sphere distribution at these densities. This suggests that the sodium cations may actually avoid each other at low densities. At the critical 20 mol% concentration and above, the initial peak exceeds what would be found in a hard-sphere distribution, with the greatest deviation at 20 mol%. Taking the hard-sphere distribution as the most random case, these data suggest that, at 20 mol% and above, the sodium cations show significant clustering, while below 20 mol% they may actually avoid each other.

6. Summary

In this paper we have reviewed recent progress in structural studies of glass, concentrating on our own work and its relation to other studies in this field. The explosive recent growth in NMR techniques for complex solids has provided a rich new set of tools for workers in this area, tools which become even more powerful when combined with complementary methods that probe different length scales. We have tried to illustrate the power of these new methods through results on three systems: borates, phosphates and tellurites.

In terms of future directions, several possibilities suggest themselves. On the methodological side, two NMR experiments appear to be critical. First, the distance measurement techniques that we have such as RFDR, while qualitatively useful, lack quantitative precision. The difficulties with modelling spin exchange in the presence of differently oriented shift tensors are serious and must be overcome if these experiments are to realize their potential. Secondly, the MQMAS experiment is currently undergoing intensive development; it has the potential of replacing DOR and DAS as the experiment of choice but has not reached that stage yet, especially for glasses where its resolution is often disappointing compared with DAS. It is not clear why this should be, but we and the others have observed this. However, once the multiple-quantum transitions are fully understood and controlled, this experiment is likely to be of great utility in glass studies.

Finally, in terms of materials science, as opposed to methods development, it now seems clear that the methodological tools are developed to the point where a new generation of studies of the relation of atomic scale structure to bulk properties of glasses appear feasible. Hopefully the sophisticated structural measurements that we can now make will shortly lead to breakthroughs in understanding practical materials properties.

Acknowledgements

It is a pleasure to thank my students and post-doctoral associates over the last few years, including Randy Youngman, Kaj Olsen, Sandra Tagg, Marco Braun, Peter Hartmann, Jay McLaughlin, John VerBurg, Kevin Smith, Brian Cherry, Erin Becker and Jeremy Wise, without whom this work would not have been possible. I also wish to thank numerous colleagues, including John Huffman, Brad Chmelka, Mike Janicke, Scott Haubrich, David Price, Yaspal Badyal, Christian Jäger, Robert McGreevy and Laszlo Pusztai. Finally, it is as always a pleasure to thank Ulrike Werner-Zwanziger for many helpful discussions.

This research was supported by the National Science Foundation under grants DMR-9115787 and DMR-9508625.

References

[1] Elliott, S. R., 1991, *Nature*, **354**, 445.
[2] Elliot, S. R., 1990, *Physics of Amorphous Materials*, second edition (New York: Wiley).
[3] Moynihan, C. T., and Schroeder, J., 1993, *J. non-crystalline Solids*, **160**, 52.
[4] Adam, G., and Gibbs, J. H., 1965, *J. chem. Phys.*, **43**, 139.
[5] Cohen, M. H., and Grest, G. S., 1979, *Phys. Rev. B*, **20**, 1077.
[6] Götze, W., 1989, *Liquids, Freezing, and the Glass Transition*, edited by J. P. Hansen and D. Levesque (New York: Plenum).
[7] Kivelson, S. A., *et al.*, 1994, *J. chem. Phys.*, **101**, 2391.
[8] Malugani, J., *et al.*, 1975, *Mater. Res. Bull.*, **13**, 427.
[9] Martin, S. W., 1989, *Mate. chem. Phys.*, **23**, 225.
[10] Moynihan, C. T., Balitactac, N., Boone, L., and Litovitz, T., 1971, *J. chem. Phys.*, **55**, 3013.
[11] Wicks, J. D., *et al.*, 1995, *Phys. Rev. Lett.*, **74**, 726.
[12] Wicks, J. D., 1993, PhD Thesis, University of Oxford, Oxford.
[13] Haeberlen, U., 1976, *High Resolution NMR in Solids: Selective Averaging*, Advances in Magnetic Resonance, Vol. Suppl. 1 (New York: Academic Press).
[14] Samoson, A., Sun, B., and Pines, A., 1992, *Pulsed Magnetic Resonance: NMR, ESR, and Optics*, edited by D. M. S. Bagguley (Oxford University Press).
[15] Chmelka, B. F., and Zwanziger, J. W., 1994, *Solid State NMR IV*, NMR Basic Principles and Progress, Vol. 33, edited by B. Blümich and R. Kosfeld (Berlin: Springer), pp. 79–124.
[16] Murdoch, J. B., Stebbins, J. F., and Carmichael, I. S. E., 1985, *Am. Mineral.*, **70**, 332.
[17] Dupree, R., Holland, D., and Williams, D. S., 1986, *J. non-crystalline Solids*, **81**, 185.
[18] Dupree, R., Holland, D., and Mortuza, M. G., 1990, *J. non-crystalline Solids*, **116**, 148.
[19] Turner, G. L., Smith, K. A., Kirkpatrick, R. J., and Oldfield, E., 1986, *J. Magn. Reson.*, **70**, 408.
[20] Hayashi, S., and Hayamizu, K., 1989, *J. solid-st. Chem.*, **80**, 195.
[21] Zhang, P., *et al.*, 1996, *J. non-crystalline Solids*, **204**, 294.
[22] Frydman, L., *et al.*, 1992, *J. Chem. Phys.*, **97**, 4800.
[23] Lee, Y. K., *et al.*, 1995, *J. Magn. Reson.* A, **112**, 112.
[24] Zwanziger, J. W., Olsen, K. K., and Tagg, S. L., 1993, *Phys. Rev.* B, **47**, 14618.
[25] Slichter, C. P., 1989, *Principles of Magnetic Resonance*, third edition. (New York: Springer).
[26] Jäger, C., 1993, NMR Basic Principles and Progress, Vol. 31, edited by B. Blümich and R. Kosfeld (Berlin: Springer), pp. 135–170.
[27] Samoson, A., Lippmaa, E., and Pines, A., 1988, *Molec. Phys.*, **65**, 1013.

[28] SAMOSON, A., and PINES, A., 1989, *Rev. scient. Instrum.*, **60**, 3239.
[29] CHMELKA, B. F., *et al.*, 1989, *Nature*, **339**, 42.
[30] WU, Y., SUN, B., and PINES, A., 1990, *J. Magn. Reson.*, **89**, 297.
[31] LLOR, A., and VIRLET, J., 1988, *Chem. Phys. Lett.*, **152**, 248.
[32] MUELLER, K. T., *et al.*, 1990, *J. Magn. Reson.*, **86**, 470.
[33] GRANDINETTI, P. J., *et al.*, 1993, *J. Magn. Reson.* A, **103**, 72.
[34] GOLDMAN, M., *et al.*, 1992, *J. chem. Phys.*, **97**, 8947.
[35] FRYDMAN, L., and HARWOOD, J. S., 1995, *J. Am. chem. Soc.*, **117**, 5367.
[36] MEDEK, A., HARWOOD, J. S., and FRYDMAN, L., 1995, *J. Am. chem. Soc.*, **117**, 12779.
[37] YOUNGMAN, R. E., WERNER-ZWANZIGER, U., and ZWANZIGER, J. W., 1996, *Z. Naturf.* (a), **51**, 321.
[38] HWANG, S.-J., *et al.*, 1997, *Solid State NMR*, **8**, 109.
[39] VAN VLECK, J. H., 1948, *Phys. Rev.*, **74**, 1168.
[40] ABRAGAM, A., 1961, *Principles of Nuclear Magnetism* (Oxford University Press).
[41] HAASE, J., and OLDFIELD, E., 1993, *J. Magn. Reson.* A, **101**, 30.
[42] GEE, B., and ECKERT, H., 1995, *Solid State NMR*, **5**, 113.
[43] YAP, A. T.-W., FÖRSTER, H., and ELLIOTT, S. R., 1995, *Phys. Rev. Lett.*, **75**, 3946.
[44] ZWANZIGER, J. W., MCLAUGHLIN, J. C., and TAGG, S. L., 1997, *Phys. Rev.* B, **56**, 5243.
[45] BENNETT, A. E., OK, J. H., GRIFFIN, R. G., and VEGA, S., 1992, *J. chem. Phys.*, **96**, 8624.
[46] JÄGER, C., FEIKE, M., BORN, R., and SPIESS, H. W., 1994, *J. non-crystalline Solids*, **180**, 91.
[47] BORN, R., FEIKE, M., JÄGER, C., and SPIESS, H. W., 1995, *Z. Naturf.* (a), **50**, 169.
[48] LEVITT, M. H., RALEIGH, D. P., CREUZET, F., and GRIFFIN, R. G., 1990, *J. chem. Phys.*, **92**, 6347.
[49] PRICE, D. L., and SKÖLD, K., 1986, *Neutron Scattering*, Methods of Experimental Physics, Vol. 23A, edited by K. Sköld and D. L. Price (Orlando, Florida: Academic Press), pp. 1–97.
[50] ELLISON, A. J. G., *et al.*, 1993, *J. Neutron Res.*, **1**, 61.
[51] MCGREEVY, R. L., and PUSZTAI, L., 1988, *Molec. Simul.*, **1**, 359.
[52] MCGREEVY, R. L., and HOWE, M. A., 1992, *A. Rev. Mater. Sci.*, **22**, 217.
[53] ARMAND, P., *et al.*, 1995, *Europhys. Lett.*, **29**, 549.
[54] BÖRJESSON, L., MCGREEVY, R. L., and WICKS, J., 1992, *J. Phys., Paris, IV*, **C2**, 107.
[55] ZOTOV, N., 1997, *Amorphous Insulators and Semiconductors*, NATO Advanced Study Institute Series, Series 3, High Technology, Vol. 23, edited by M. F. Thorpe and M. I. Mitkova (Dordrecht: Kluwer) p. 225.
[56] BRIL, T. W., 1976, *Philips Res. Rep. Suppl.*, **2**, 1.
[57] HANNON, A., WRIGHT, A., BLACKMAN, J., and SINCLAIR, R., 1995, *J. non-crystalline Solids*, **182**, 78.
[58] GRAVINA, S. J., and BRAY, P. J., 1990, *J. Magn. Reson.* **89**, 515.
[59] JELLISON, G. E., JR, PANEK, L. W., BRAY, P. J., and ROUSE, G. B., 1977, *J. chem. Phys.*, **66**, 802 (1977).
[60] YOUNGMAN, R. E., and ZWANZIGER, J. W., 1994, *J. non-crystalline Solids*, **168**, 293.
[61] YOUNGMAN, R. E., *et al.*, 1995, *Science*, **269**, 1416.
[62] SILVER, A. H. and BRAY, P. J., 1958, *J. chem. Phys.*, **29**, 984.
[63] UHLMANN, D., HAYS, J., and TURNBULL, D., 1967, *Phys. Chem. Glasses*, **8**, 1.
[64] TOSSELL, J. A., 1995, *J. non-crystalline Solids*, **183**, 307.
[65] YOUNGMAN, R. E., and ZWANZIGER, J. W., 1996, *J. phys. Chem.*, **100**, 16720.
[66] MOZZI, R. L., and WARREN, J., 1976, *J. appl. Crystallogr.* **3**, 251.
[67] JOHNSON, P. A. V., WRIGHT, A. C., and SINCLAIR, R. N., 1980, *J. non-crystalline Solids*, **50**, 281.
[68] SWENSON, J., and BÖRJESSON, L., 1992, *Phys. Rev.* B, **55**, 11138.
[69] FERNANDEZ-PEREA, R., BERMEJO, F. J., and SENENT, M. L., 1996, *Phys. Rev.* **54**, 6039.
[70] BOKOV, N., 1994, *J. non-crystalline Solids*, **177**, 74.
[71] WALRAFEN, G. E., SAMANTA, S. R., and KRISHNAN, P. N., 1980, *J. chem. Phys.*, **72**, 113.
[72] YOUNGMAN, R. E., and ZWANZIGER, J. W., 1995, *J. Am. chem. Soc.*, **117**, 1397.
[73] MARTIN, S. W., *et al.*, 1986, *Solid St. Ionics*, **18/19**, 421.
[74] ROOS, J., *et al.*, 1988, *Sold St. Ionics*, **28–30**, 710.
[75] OLSEN, K. K., and ZWANZIGER, J. W., 1995, *Solid State NMR*, **5**, 123.
[76] KRONENBITTER, J., SCHWEIZER, U., and SCHWENK, A., 1980, *Z. Naturf.* (a) **35**, 319.

[77] EL-MALLAWANY, R., 1992, *J. appl. Phys.*, **72**, 1774.
[78] KIM, S.-H., YOKO, T., and SAKKA, S., 1993, *J. Am. Ceram. Soc.*, **76**, 2486.
[79] NEOV, S., *et al.*, 1979, *J. Phys.*, C, **12**, 2475.
[80] HEO, J., *et al.*, 1992, *J. Am. Ceram. Soc.*, **75**, 277.
[81] LEE, S. K., TATSUMISAGO, M., and MINAMI, T., 1994, *Phys. Chem. Glasses*, **35**, 226.
[82] YOKO, T., FUJITA, M., MIYAJI, F., and SAKKA, S., 1990, *Chem. Express*, **5**, 549.
[83] SEKIYA, T., MOCHIDA, N., OHTSUKA, A., and TONOKAWA, M., 1992, *J. non-crystalline Solids*, **144**, 128.
[84] KOWADA, Y., *et al.*, 1992, *Chem. Express*, **7**, 965.
[85] TATSUMISAGO, M., MINAMI, T., KOWADA, Y., and ADACHI, H., 1994, *Phys. Chem. Glasses*, **35**, 89.
[86] LINDQVIST, O., 1968, *Acta Chem. Scand.*, **22**, 977.
[87] MASSE, R., GUITEL, J. C., and TORDJMAN, I., 1986, *Mater. Res. Bull.*, **15**, 431.
[88] HANTKE, G. (editor), 1976, *Tellur*, *Gmelin Handbuch der Anorganischen Chemie* (Berlin: Springer).
[89] TAGG, S. L., HUFFMAN, J. C., and ZWANZIGER, J. W., 1994, *Chem. Mater.* **6**, 1884.
[90] TAGG, S. L., HUFFMAN, J. C., and ZWANZIGER, J. W., 1997, *Acta Chem. Scand.*, **51**, 118.
[91] BECKER, C. R., TAGG, S. L., HUFFMAN, J. C., and ZWANZIGER, J. W., 1997, *Inorg. Chem.*, **36**, 5559.
[92] GREAVES, G. N., *et al.*, 1991, *Phil. Mag.* A, **64**, 1059.
[93] HOUDE-WALTER, S. N., INMAN, J. M., DENT, A. J., and GREAVES, G. N., 1993, *J. phys. Chem.*, **97**, 9330.
[94] HOUDE-WALTER, S. N., *et al.*, 1996, *J. non-crystalline Solids*, **194**, 85.
[95] TAGG, S. L., YOUNGMAN, R. E., and ZWANZIGER, J. W., 1995, *J. phys. Chem.*, **99**, 5111.
[96] KOLLER, H., ENGELHARDT, G., KENTGENS, A. P. M., and SAUER, J., 1994, *J. phys. Chem.*, **98**, 1544.
[97] XUE, X., and STEBBINS, J. F., 1993, *Phys. Chem. Minerals*, **20**, 297.